Optical Engineering

OpticalEngineering.SPIEDigitalLibrary.org

Practical limits of power transmission through single-mode chalcogenide fibers

Alex Sincore
Justin Cook
Felix Tan
Ayman F. Abouraddy
Martin C. Richardson
Kenneth L. Schepler

SPIE.

Alex Sincore, Justin Cook, Felix Tan, Ayman F. Abouraddy, Martin C. Richardson, Kenneth L. Schepler, "Practical limits of power transmission through single-mode chalcogenide fibers," *Opt. Eng.* **57**(11), 111807 (2018), doi: 10.1117/1.OE.57.11.111807.

Practical limits of power transmission through single-mode chalcogenide fibers

Alex Sincore,* Justin Cook, Felix Tan, Ayman F. Abouraddy, Martin C. Richardson, and Kenneth L. Schepler
University of Central Florida, CREOL, The College of Optics and Photonics, Orlando, Florida, United States

Abstract. Beam confinement or "no free-space optics" via fiber transmission can achieve improved reliability, lower cost, and reduced component count for active sensing systems. For midinfrared delivery, mechanically robust chalcogenide (arsenic sulfide) single-mode fibers are of interest. A 12-μm core diameter fiber is shown to transport >10 W at 2053 nm, and a 25-μm core diameter fiber enables single-mode beam transport from a 4550-nm quantum cascade laser. As midinfrared sources continue to increase their output power capabilities, chalcogenide fibers will eventually be limited in their power-handling capacity due to optical nonlinearities or thermal failure. These limitations are discussed and analyzed in the context of single-mode chalcogenide fibers in order to provide a framework for power transmission limitations in various operating regimes. © *2018 Society of Photo-Optical Instrumentation Engineers (SPIE)* [DOI: 10.1117/1.OE.57.11.111807]

Keywords: optics; fibers; chalcogenide glass; lasers; infrared; nonlinear.

Paper 180627SS received May 1, 2018; accepted for publication Oct. 23, 2018; published online Nov. 19, 2018.

1 Introduction

Midinfrared (MIR) applications in remote sensing, medical, and defense are under rapid development. Key to these applications is lasers and frequency conversion devices capable of generating wavelengths throughout the 2- to 12-μm range. MIR transition-metal solid-state sources, specifically Cr:ZnSe and Fe:ZnSe, have demonstrated high average powers and broadband wavelength tunability.[1] Rare-earth solid-state sources have been efficiently frequency converted to the MIR.[2] MIR fiber sources are also experiencing improvements, with output powers of 30 W at 2.94 μm and 5 W at 3.55 μm.[3,4] Compact and efficient quantum cascade lasers (QCL) can generate over 1 W throughout the 3.8- to 10.7-μm range.[5]

As all of these MIR sources continue to develop, there will be a need to deliver these high power sources to the application site as well as collect the scattered and re-emitted light. For infrared sensing systems, free-space elements that direct MIR radiation to a detector, or aim the source beams to a target, can be replaced by fiber optics with considerable improvement in size, weight, and cost of the system as well as increased reliability. For many of these applications, the MIR fiber optics must deliver high power beams several meters to a target location. Silica fibers suffer high propagation loss beyond 2.5 μm, requiring the use of heavy glasses to push off the multiphonon absorption edge to enable MIR fiber delivery. Common glasses used for delivering MIR radiation are tellurite, germanate, ZBLAN, and chalcogenide (ChG).[6]

Advances in ChG fiber development are rapidly evolving in areas of all-fiber sensing,[7–9] nonlinear supercontinuum generation,[10–13] ultralow loss fabrication,[14,15] and even rare-earth doped ChG fibers.[16–18] While ChG fibers enable some of the broadest transmission windows in the MIR (1 to 12 μm depending on ChG composition), they can suffer from poor mechanical robustness for practical use. By utilizing a multimaterial hybrid fiber fabrication process, low-loss and mechanically robust ChG fibers have been drawn.[19] For the intended applications of high power MIR delivery, near diffraction-limited beam quality is preferred and/or required. Therefore, the ChG fibers presented here were designed and fabricated for coupling and delivery of single-mode beams. The fabrication method and preliminary characterization have been reported by Shabahang et al.,[19] and high power coupling of various MIR sources was described by Sincore et al.[20]

Here, we briefly describe the ChG test fibers and transmission tests at 2053 and 4550 nm in Sec. 2. As previously reported, the input uncoated facet sustained 12 MW/cm^2 without failure from a 2053-nm source, and an antireflection (AR)-coated fiber transmitted 10.3 W with 90% transmission.[20] However, the primary limitation for higher power transmission was damage to the AR coatings on the fiber facets. Improving the AR-coatings or utilizing AR microstructures will enable higher power handling capabilities.[21]

Nonetheless, high power transmission will ultimately be limited by optical nonlinearities and/or thermal failure. These limiting mechanisms are addressed and discussed in Sec. 3. Theoretical calculations show that stimulated Brillouin scattering (SBS) will limit power handling of single-frequency sources to ~1 W through a few meters of fiber while stimulated Raman scattering (SRS) becomes problematic for >100 W delivery. Thermal failure due to heating of the ChG glass material is also investigated. As expected, ultralow loss fibers are necessary to prevent thermal failure for ~100-W power delivery in an ambient environment. Lastly, these power transmission limitations are summarized for various operating regimes to provide a framework for future high power MIR delivery in ChG fibers.

*Address all correspondence to: Alex Sincore, E-mail: asincore@knights.ucf.edu

Fiber diameter	ChG-A	ChG-B
ChG core	12 μm	25 μm
ChG cladding	145 μm	310 μm
PEI coating	700 μm	920 μm

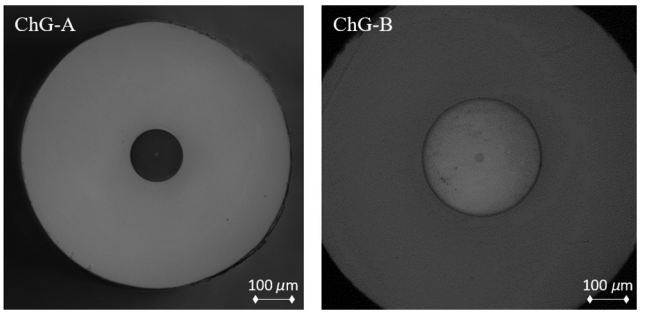

Fig. 1 Dimensions of the in-house drawn chalcogenide fibers and optical images of the flat polished facets.

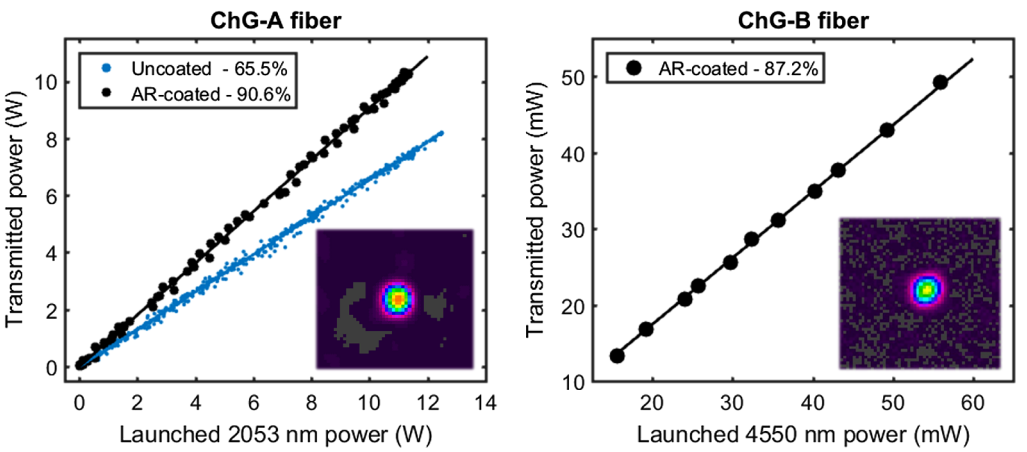

Fig. 2 The uncoated ChG-A fibers sustains ~12 MW/cm^2 intensities on the facet without failure. AR-coating the fiber enables high transmission and 10.3 W delivery through a 20-cm length. The ChG-A results were first published in Ref. 20. The AR-coated ChG-B fiber enables coupling and delivery of highly divergent QCL radiation.

2 Single-Mode Chalcogenide Fibers and Measured Beam Delivery

The in-house ChG fibers tested, as well as the fibers theoretically investigated for power handling limitations, are based on arsenic sulfide glasses (As_2S_3). As such, the "ChG" abbreviation implies arsenic-sulfide-based chalcogenide fibers for the remaining discussion. Low numerical aperture (NA) ChG fibers are typically in the range of NA $\approx$ 0.2 to 0.3, limited by the difference in arsenic composition between the core and cladding glasses.[22–24] Since unwanted optical nonlinearities and damage processes scale with intensity, large core diameters are desired. However, we limit further discussion here to single-mode fiber where high beam quality can be maintained. Large core diameter single-mode fibers would require lower core NAs than currently available or complex fiber geometries such as photonic crystal fibers.[25,26] As such, the ChG fibers drawn in-house were fabricated with a core and cladding composition of $As_{39}S_{61}$ and $As_{38.5}S_{61.5}$, resulting in a core NA of ~0.2. The ChG fibers were produced via a hybrid multimaterial thermal drawing process as described with detail in Ref. 19.

Two ChG fibers were drawn: a 12-μm core diameter fiber for short-wavelength operation, henceforth labeled ChG-A; and a 25-μm core diameter fiber for long-wavelength operation, labeled ChG-B. Optical images of the polished fiber facets are shown in Fig. 1, along with the fiber dimensions. The large polyetherimide (PEI) jacket provides excellent mechanical robustness as compared to the poor handling properties of standard ChG fibers. Background loss measurements indicate an upper-limit of 0.95 and 1.1 dB/m at 2.0 and 4.6 μm, respectively.[19] While these losses are significantly higher than silica, these values are typical for ChG fibers. With ideal glass and fiber preparation, ChG fibers can be drawn with losses of ~0.1 dB/m or lower.[15,27]

Power handling and single-mode beam delivery of the ChG-A fiber was performed using a >15-W average power, 2053-nm, thulium-doped fiber laser.[28] The high power handling results for the ChG-A fiber were presented in Ref. 20. In summary, uncoated ChG-A fibers could withstand the full power without failure, suggesting polished facets can reliably sustain ~12 MW/cm^2 intensities. This was also recently demonstrated by Chenard et al.[29] in which 6.9 W was incident on a 9-μm core diameter ChG fiber. Furthermore, a 20-cm length AR-coated fiber demonstrated >90% transmission, enabling 10.3 W through the fiber. Figure 2 shows these results and shows the single-mode output beam profile.

For the ChG-B fiber, the capability to couple and deliver a highly divergent QCL at 4550 nm was investigated. The Fabry–Perot QCL had a slow-axis and fast-axis FWHM divergence of 60 deg and 110 deg, respectively. An in-house designed telescope utilizing commercial-off-the-shelf lenses

was used to couple the QCL radiation into a 20-cm length AR-coated ChG-B fiber. Attempting to couple into an uncoated fiber caused undesirable fluctuations of the QCL output due to backreflections off the ChG facet, which forms a cavity coupled with the QCL resonator cavity. As shown in Fig. 2, 50 mW was coupled and transmitted through the AR-coated ChG-B fiber with 87% efficiency and single-mode beam quality. These results demonstrate the capability to efficiently restructure the highly astigmatic and divergent QCL output beam and couple into a single-mode fiber for versatile MIR delivery.

For the AR-coated ChG fibers, the Al_2O_3 thin-film coatings experienced cracking after deposition due to differences in their coefficient of thermal expansion compared to the PEI jacket. After high power exposure, the AR-coating of the ChG-A fiber exhibited additional cracking and discoloration at the input core region. Therefore, the limiting factor in higher power handling for these particular AR-coated ChG fibers was the Al_2O_3 coating. For the ChG-B fiber, higher power transmission is currently limited by the QCL output power. As MIR sources continue to improve in output power and brightness, ChG fibers will become limited in their power handling capacity. Determining these power handling limits is the focus of Sec. 3.

3 Limitations in High Power, Single-Mode Delivery Through ChG Fiber

From the experimental results presented above and in Ref. 20, damage to the AR-coated facets was the primary limitation for further power scaling. Uncoated fibers could withstand 12.5-W incident on the input facet without failure. Improvements in the AR-coating are required for high power transmission while maintaining low reflections at each facet. Another promising avenue is AR microstructures,[21] which eliminates the need to match the ChG glass and AR-coating coefficients of thermal expansion. Furthermore, the damage threshold of the AR microstructures is expected to be equal to or greater than the damage threshold of the ChG glass itself. Damage threshold testing with 2.1 μm, 80 ns pulses measured 2.5 J/cm^2 for uncoated As_2S_3 windows, and 3.5 J/cm^2 for microstructured As_2S_3 windows.[30]

Damage thresholds for CW operation are not readily available in the literature but the results from Sec. 2 and Ref. 29 indicate that 12 MW/cm^2 can be handled by a polished fiber facet. Use of a high-quality AR structure and endcaps (to increase the area of the beam at the air-fiber surface) can significantly increase the power handling of ChG facets. For example, an endcap that permits use of a 100-μm-diameter incident beam theoretically indicates nearly 1 kW of average power can be handled. Experimentally, a highly multimode 1-mm core diameter fiber withstood over 400 W.[31] However, higher power handling of single-mode ChG fibers will eventually be limited by either optical nonlinearities or thermal failure. The power thresholds for these various processes are discussed and compared below for the ChG-A and ChG-B fibers.

3.1 *Stimulated Brillouin Scattering*

SBS is a nonlinear interaction between an optical pump wave and an acoustic phonon. The SBS Stokes frequency shift induced by acoustic scattering in As_2S_3 chalcogenide glass is ~8 GHz at $\lambda = 1550$ nm.[32,33] For such a small frequency shift, it can be shown that the scattered Stokes wave travels in the backward direction through an optical fiber.[34] For this reason, SBS is a detrimental nonlinearity because it will scatter a large fraction of the optical power back toward the input, damaging the source and/or any components. Fortunately, the Brillouin gain bandwidth is very narrow, measured to be 34 MHz at $\lambda = 1545$ nm in an As_2S_3 ridge waveguide.[35] This means only narrow-linewidth, single-frequency sources suffer SBS. If a source linewidth is broad, then the onset of SBS is increased by approximately the ratio of the source linewidth to the Brillouin gain bandwidth.

Calculation of the theoretical SBS thresholds for both ChG-A and ChG-B fibers used the full derivation provided by Kobyakov et al.[36] The derivation assumes the initial SBS Stokes power originates from thermally populated spontaneous phonons. The derivation also uses the undepleted pump approximation to analytically solve the coupled differential equations. This analytical solution for the SBS threshold is given by the following transcendental equation:

$$P_{\mathrm{SBS}} = \frac{1}{\mu}\frac{4\pi}{3}\Theta e^{q/2}\left\{q\left(1+\frac{e^{-\alpha L}}{2}\right)\left[I_0\left(\frac{q}{2}\right)-I_1\left(\frac{q}{2}\right)\right] - (1-e^{-\alpha L})I_1\left(\frac{q}{2}\right)\right\}, \tag{1}$$

where

$$q = \frac{g_B P_{\mathrm{SBS}}}{A_{\mathrm{eff}}} L_{\mathrm{eff}}, \tag{2}$$

$$L_{\mathrm{eff}} = \frac{(1-e^{-\alpha L})}{\alpha}, \tag{3}$$

$$\Theta = \frac{kT\nu_p w_B}{2\nu_B}. \tag{4}$$

Here I_l is the modified Bessel function of order l, L is the fiber length, g_B is the Brillouin gain coefficient, A_{eff} is the optical mode area, α is the propagation loss, v_B is the Brillouin frequency shift, v_p is the pump frequency, w_B is the Brillouin gain bandwidth, k is the Boltzmann's constant, and T is the temperature.[36] The term μ is the ratio of pump power scattered into the SBS Stokes wave. Because the undepleted pump approximation was used in the derivation, it is ideal to keep $\mu < 0.1$ for accuracy. For practical systems, $\mu < 0.01$ to prevent system damage from backreflections.

Table 1 summarizes the input parameters used to calculate the SBS thresholds. The ChG-A fiber is used to guide a 2053-nm source while the ChG-B fiber guides 4550 nm. The SBS frequency shift and gain bandwidth vary with wavelength and are considered in the analyses. Also, propagation losses of both 0.1 and 1.0 dB/m are theoretically examined, corresponding to ultralow loss and typical loss fibers.

The onset of SBS is primarily affected by the Brillouin gain coefficient and fiber length. The Brillouin gain coefficient for As_2S_3 glass has been both theoretically and experimentally calculated, ranging from 0.48 to 3.9 nm/W.[32,33,35]

Table 1 Fiber parameters used for determining SBS thresholds of the single-mode ChG fibers.

Parameter	Unit	ChG-A	ChG-B	Reference/comment
Wavelength	nm	2053	4550	
Mode radius	μm	5.3	11.2	
Fiber loss	dB/m	0.1 and 1.0	0.1 and 1.0	
Brillouin gain coefficient	nm/W	0.48 and 3.9	0.48 and 3.9	Refs. 32 and 33
Brillouin gain bandwidth	MHz	19.3	3.9	Ref. 35 using λ^{-2} dependency
Brillouin frequency shift	GHz	6.0	2.7	Ref. 33 using λ^{-1} dependency
SBS threshold definition	%	1	1	With respect to input power

ChG fibers are known to have higher nonlinear gain compared to silica fibers. For comparison, silica fibers range from 0.01 to 0.05 nm/W.

Using these parameters, the SBS thresholds for the two ChG fibers are calculated and shown in Fig. 3. The SBS threshold can be approximated using the commonly used expression given by Eq. (5),[37] where C_{SBS} is a unitless constant:

$$P_{\mathrm{SBS}} \approx C_{\mathrm{SBS}} \cdot \frac{A_{\mathrm{eff}}}{g_B L_{\mathrm{eff}}}. \tag{5}$$

Typically, a factor of $C_{\mathrm{SBS}} = 21$ is used for silica fibers from Smith's derivation.[37] For these ChG fiber parameters, a factor of ~15 to 19 matches the numerical derivations. For the approximation in Fig. 3, a factor $C_{\mathrm{SBS}} = 17$ was used and matched both fibers well.

The SBS threshold calculations indicate a ~1.9-W SBS threshold for a 20-cm length ChG-A fiber if the Brillouin gain coefficient is 3.9 nm/W. However, as shown in Fig. 2, ~11 W was transmitted through 20 cm utilizing a single-frequency source ($\Delta\nu_L \approx 600$ kHz). During these experiments, no indication of SBS was observed and no power rollover occurred. This suggests that the Brillouin gain coefficient is toward the lower reported value. If the Brillouin gain coefficient is 0.48 nm/W, then the SBS threshold is higher at ~17 W and would not have been observed in the experiments from Sec. 2.

For a fiber transport system, the key metric is the delivered power at the fiber output. Therefore, it is more informative to plot the transmitted power at the SBS threshold. This is given as

$$P_{\mathrm{out}} = P_{\mathrm{SBS}}(e^{-\alpha L} - \mu), \tag{6}$$

where P_{SBS} is the calculated SBS threshold from Eq. (1). Figure 4 shows the transmitted power at the SBS threshold versus fiber length for the parameters previously used. The main point provided by Fig. 4 is that the SBS threshold is very low for small core diameter fibers such as ChG-A. The SBS threshold is approximately 5× higher for the ChG-B fiber. This is primarily because the fiber's optical mode area is correspondingly ~4.5× larger. Mode area scaling with wavelength is a well-known advantage to mitigate nonlinearities in fibers. Presuming the Brillouin gain coefficient is 0.48 nm/W at the low end of the reported range, the ChG-B fiber can transmit over 1 W from a single-frequency source for 10 m if the fiber loss can be kept low. At longer fiber lengths, the higher loss raises the SBS threshold but also decreases the net power transmission. This is the reason for the downward curvature of the transmitted power plots at long fiber lengths.

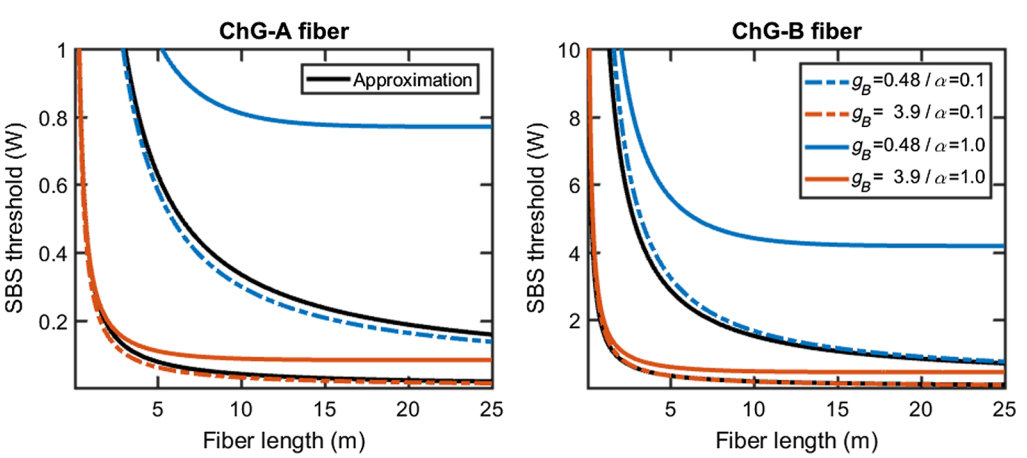

Fig. 3 Numerically calculated SBS thresholds using Eq. (1) and the simplified approximation from Eq. (5). The parameters listed in Table 1 were used for the calculations. The Brillouin gain coefficient, g_B, is units of nm/W and the fiber loss, α, is units of dB/m.

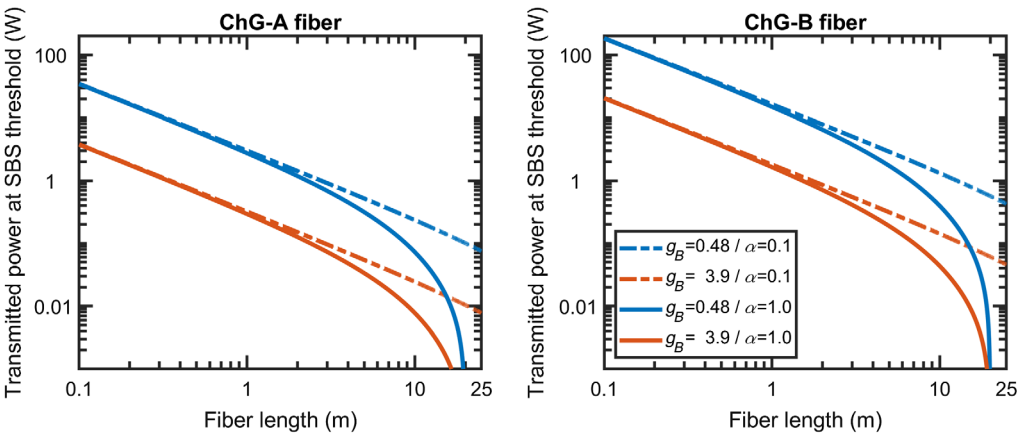

Fig. 4 Calculated output power at the SBS thresholds using Eq. (6) for the two ChG fibers. The Brillouin gain coefficient, g_B, is units of nm/W and the fiber loss, α, is units of dB/m.

3.2 *Stimulated Raman Scattering*

SRS is a nonlinear interaction between an optical pump wave and an optical phonon. The frequency shift induced by Raman is much larger than SBS and is ~10.3 THz in As_2S_3 chalcogenide glass.[38,39] SRS is undesirable because it converts the initial wavelength into a separate redshifted wavelength, which may not be useable for the intended application. As such, SRS should be avoided during fiber transmission. The SRS gain bandwidth in As_2S_3 is ~2.7 THz,[38] and therefore will affect transmission of any typical laser. Similar to SBS, ChG fibers are known to have higher Raman gain compared to silica fibers. The Raman gain coefficient for As_2S_3 glass has been measured to be around 4.4 to 5.7 pm/W at $\lambda = 1550$ nm.[38,39] In comparison, silica fibers range from 0.06 to 0.11 pm/W at $\lambda = 1550$ nm.[40,41]

In order to calculate the theoretical SRS thresholds for both ChG-A and ChG-B fibers, the well-known analysis provided by Smith is used.[37] The SRS process is conjectured to originate from amplified spontaneous Stokes emission throughout the fiber length. This "input noise" is equivalent to seeding with an effective Stokes power given by Eq. (8). The derivation also uses the undepleted pump approximation to analytically solve the coupled differential equations. This analytical solution for the SBS threshold is given by the following transcendental equation:

$$P_{\mathrm{SRS}} = \frac{1}{\mu} \cdot \frac{P_0 \cdot \exp\left(P_{\mathrm{SRS}} \frac{g_R L_{\mathrm{eff}}}{A_{\mathrm{eff}}} - \alpha L\right)}{e^{-\alpha L}}, \tag{7}$$

where

$$P_0 = h\nu_s \frac{\sqrt{\pi}}{2} \frac{\mathrm{w}_R}{\sqrt{\frac{P_{\mathrm{SRS}}}{A_{\mathrm{eff}}} g_R L_{\mathrm{eff}}}}. \tag{8}$$

Here, P_0 is the input noise power, g_R is the Raman gain coefficient, w_R is the Raman gain bandwidth, v_s is the Stokes frequency, and h is Planck's constant.[37] The remaining terms were defined in Sec. 3.1 for the SBS threshold derivation. The fiber loss is assumed the same for both the pump and Stokes frequency. The term μ is the ratio of pump power scattered into the forward SRS Stokes wave. Because the undepleted pump approximation was used in the derivation, it is ideal to keep $\mu < 0.1$ for accuracy.

Table 2 summarizes the input parameters used to calculate the SRS thresholds. The ChG-A fiber is used to guide a 2053-nm source while the ChG-B fiber guides 4550 nm. In contrast to SBS, the Raman gain coefficient varies with wavelength and is considered in the analyses. The average Raman gain coefficient from Refs. 38 and 39 is used. Lastly, propagation losses of both 0.1 and 1.0 dB/m are examined.

Table 2 Fiber parameters used for determining SRS thresholds of the single-mode ChG fibers.

Parameter	Unit	ChG-A	ChG-B	Reference/comment
Wavelength	nm	2053	4550	
Mode radius	μm	5.3	11.2	
Fiber loss	dB/m	0.1 and 1.0	0.1 and 1.0	
Raman gain coefficient	pm/W	3.8	1.7	Refs. 38 and 39 using λ^{-1} dependency
Raman gain bandwidth	THz	2.7	2.7	Ref. 38
Raman frequency shift	THz	10.3	10.3	Refs. 38 and 39
SRS threshold definition	%	1	1	With respect to input power

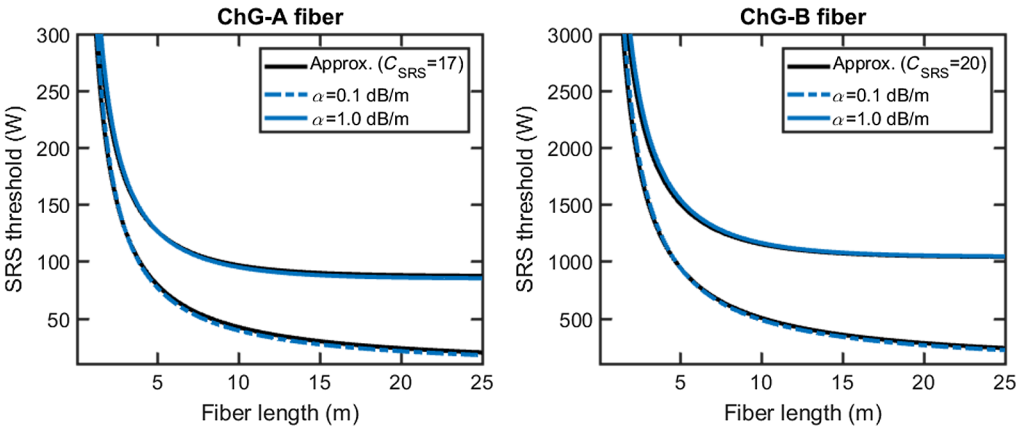

Fig. 5 Numerically calculated SRS thresholds using Eq. (7) and the simplified approximation from Eq. (9). The parameters listed in Table 2 were used for the calculations.

Using these parameters, the SRS thresholds for the two ChG fibers are calculated and shown in Fig. 5. The SRS threshold can also be approximated by the same expression as the SBS threshold, which is given as

$$P_{\mathrm{SRS}} \approx C_{\mathrm{SRS}} \cdot \frac{A_{\mathrm{eff}}}{g_R L_{\mathrm{eff}}}. \tag{9}$$

Typically, a factor of $C_{\mathrm{SRS}} = 16$ is used for silica fibers from Smith's derivation.[37] Unlike the SBS thresholds, one value for C_{SRS} does not match both fibers. For these ChG fiber parameters, it is found that a factor of ~17 matches the numerical derivations for the ChG-A fiber, but a larger factor of ~20 is required for the ChG-B fiber. This is because of the longer wavelength and its impact on the numerical derivation.

Figure 6 shows the power transmitted through the fiber at the SRS threshold determined using Eq. (6) similar to the SBS analysis. Because the Raman gain coefficient is lower by orders of magnitude than the Brillouin gain coefficient, SRS is not as significant a limitation. For a 20-cm length ChG-A fiber, the SRS threshold is over 2 kW. Clearly, SRS should not be observed in short-length ChG fibers, whereas for fibers >10 m in length transmission is limited to under 50 W.

The SRS threshold is over 10× higher for the ChG-B fiber at 4.55 μm. This is because the Raman gain coefficient decreases with wavelength; and the fiber's optical mode area is larger by ~4.5×. Both of these scaling factors combined provide a ~10× increase in the SRS threshold. This is beneficial for long wavelength MIR fiber delivery.

Overall, the SRS threshold is clearly much higher than the SBS threshold. If the source linewidth is >100× broader than the SBS gain bandwidth (≫1 GHz), then SBS will not be observed while SRS will be the limiting factor for power levels in the 100-W regime for short-length fiber transmission. Given a 0.1-dB/m loss, over 50 W can be transmitted through a 10-m ChG-A fiber and nearly 500 W can be transmitted through a ChG-B fiber.

3.3 *Thermal Failure*

While the SBS and SRS nonlinearities will limit power handling through single-mode ChG fibers, thermal limitations also need to be considered. ChG glass has a significantly lower glass transition temperature than silica, ~180°C to 200°C for As_2S_3 glass.[42,43] The upper use temperature for As_2S_3 is thus recommended to be 150°C.[43] In order to determine the power required to reach thermal failure, COMSOL was used to solve the temperature profile across the fiber.

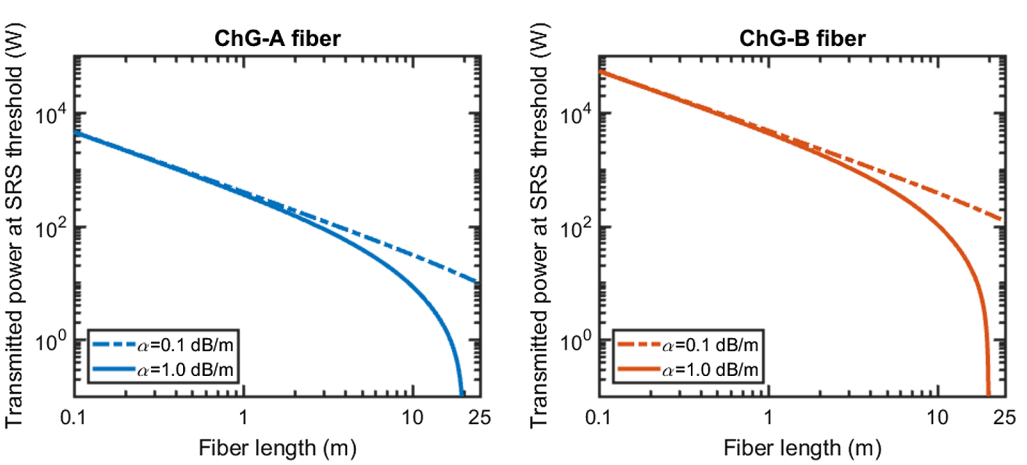

Fig. 6 Calculated output power at the SRS thresholds using Eq. (6) for the two ChG fibers. SRS limits attainable output powers much less than SBS when compared to Fig. 4.

Table 3 Fiber parameters used for determining thermal failure thresholds of the single-mode ChG fibers.

Parameter	Unit	ChG-A	ChG-B	Reference/comment
Heat source diameter	μm	10.6	22.5	Gaussian profile
As_2S_3 diameter	μm	145	310	Glass cladding diameter
PEI diameter	μm	700	920	Polymer coating diameter
Fiber loss	dB/m	0.1 and 1.0	0.1 and 1.0	
As_2S_3 thermal conductivity	W/(m·K)	0.17	0.17	Refs. 42 and 43
PEI thermal conductivity	W/(m·K)	0.22	0.22	Ref. 44
Heat transfer coefficient to surroundings	$W/(m^2 \cdot K)$	1 to 5000	1 to 5000	Stagnant to forced air cooling

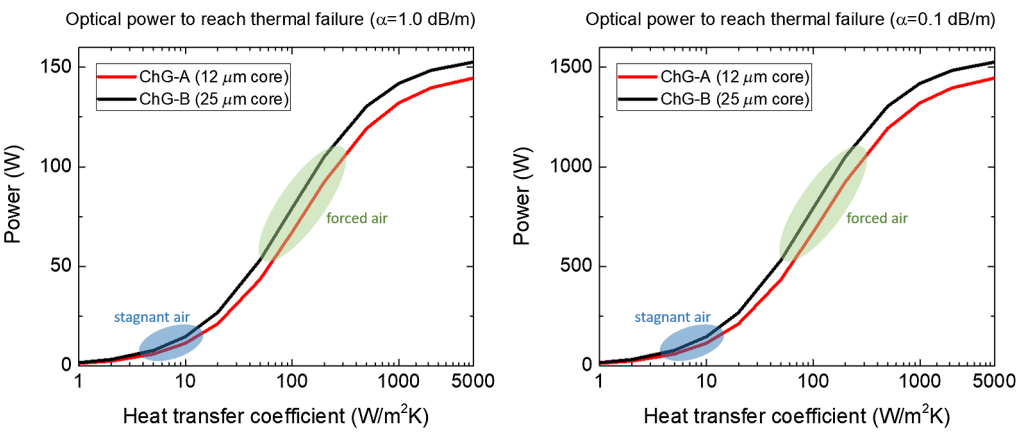

Fig. 7 The optical power required to reach thermal failure of the ChG fibers with two different propagation losses. Thermal failure is when the As_2S_3 glass reaches 150°C. Approximate heat transfer coefficient values for stagnant and forced air-cooling are shown. An infinite heat transfer coefficient corresponds to clamping the outer cylindrical PEI surface to ambient temperature.

Thermal failure was defined as when the ChG material reaches 150°C. Heating of the ChG fiber originates from background loss, and therefore low loss fibers offer a significant advantage. Table 3 summarizes the parameters used to model the temperature distribution across the ChG fibers. Not only is the low failure temperature an issue for ChG fibers but also the thermal conductivity is low at $\sim 0.17\ W/(m \cdot K)$.[42,43] The PEI polymer jacketing is similar at $\sim 0.22\ W/(m \cdot K)$[44] but has a higher failure temperature near 170°C.[45] Also, the PEI jacket will have lower temperatures than the maximal temperature because it is located away from the heat source at the core.

Figure 7 shows the power required to reach thermal failure with respect to the heat transfer coefficient. It is clear that reducing the background loss is critical to enable high power delivery in ChG fibers. For a background loss of 1.0 dB/m, the ChG-A fiber can only withstand ~5 to 10 W in stagnant air. As shown in Sec. 2, the ChG-A fiber withstood >10 W without cooling. It should be noted that the first few centimeters were in direct contact with an aluminum v-groove, which would facilitate heat extraction. Furthermore, the measured losses of ~1.0 dB/m are an upper-limit and the actual losses are likely lower. If the losses are 0.1 dB/m, the ChG fibers can withstand >50 W in stagnant air and >500 W with forced air-cooling. This is important in regards to active sensing systems in which it would be beneficial to house the fibers without any need for cooling.

Doubling the core radius results in a calculated ~12% increase in power handling. Any further increase in core diameter is not practical because the fiber will no longer be single-mode. Varying the PEI jacket diameter can provide an increase in power handling before thermal failure. Figure 8 shows the effect of varying the polymer jacket thickness for fibers with low loss of 0.1 dB/m. For low heat transfer coefficients, a larger diameter is advantageous as it provides more surface area to extract heat. However, for very high heat transfer coefficients, smaller diameters are beneficial. The inflection point is related to the thermal conductivity of the various fiber components. For common ChG fibers and common cooling methods, it will typically be beneficial to increase the overall diameter. Although, increasing the diameter beyond several millimeters will begin to restrict the fiber's flexibility.

For fibers housed in stagnant air, a considerable ~3.5× increase in power handling can be realized by quadrupling the PEI jacket diameter from 400 μm to 1.6 mm but with the expense of flexibility. For air-cooled fibers (higher heat transfer coefficients), this power handling benefit diminishes. If the thermal conductivity of the polymer jacketing could be increased, this would benefit the thermal properties

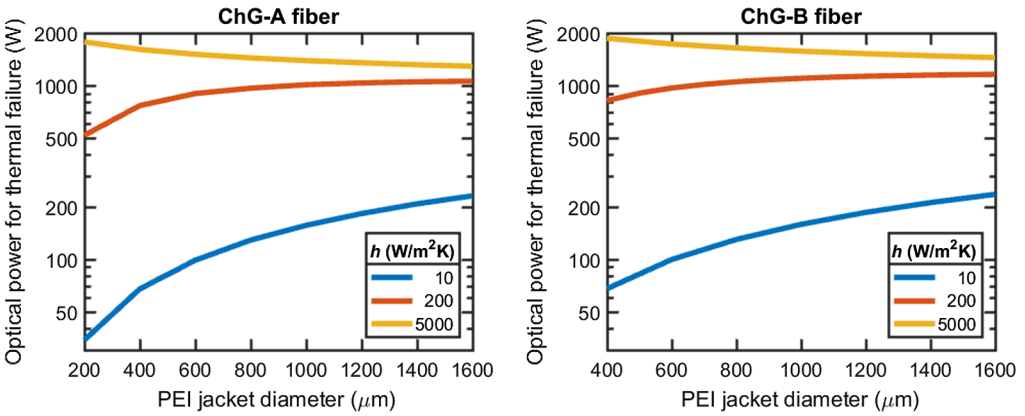

Fig. 8 The optical power required to reach thermal failure for low-loss ChG fibers for various PEI jacket thicknesses. Heat transfer coefficients representing stagnant air ($h = 10$), forced air ($h = 200$), and direct cooling ($h = 5000$) are illustrated. Thermal failure is when the As_2S_3 glass reaches 150°C.

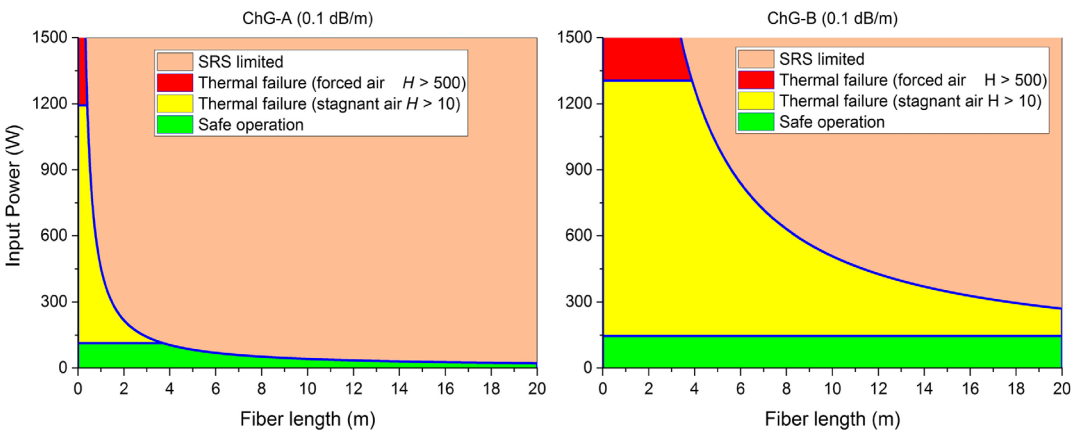

Fig. 9 Power handling regimes for the two ChG fibers considering low propagation loss and assuming a broad laser linewidth to avoid SBS. Thermal failure is the primary constraint for a fiber in stagnant air. For small-core ChG fibers (operation at shorter wavelengths), SRS will become a primary limitation if forced air cooling is applied.

without having to affect the overall fiber diameter. Improvements in coating technology or adding conductive fillers would benefit this area.[44]

3.4 *Summary of Limitations for High Power ChG Fiber Delivery*

Figure 9 shows a summary of which optical and thermal effects are dominant for various combinations of input power and chalcogenide fiber. Figure 9 considers only the case where SBS is not dominant, i.e., where the spectral linewidth of the input beam is much greater than the Brillouin gain bandwidth (≫1 GHz). Differences in core diameter (prime factor) and propagating wavelength (secondary factor) contribute major changes to the power and fiber length limits of SRS onset. Heating is the primary limit where SRS is not a factor. The thermal limit depends critically on the heat transfer rate. Minimal air-cooling should allow safe operation for 50 W of power. Larger core sizes and/or improved heat removal should allow power transport of hundreds of watts.

Not shown in these plots is the effect of surface damage. Previous performance testing has always shown that surface damage was the limiting factor for AR-coated fibers. However, as mentioned in Sec. 3 introduction, use of end caps and AR microstructures is likely to increase surface total power handling by orders of magnitude; a change of incident beam diameter from 10 to 100 μm results in a 100× increase in total power for the same power density. Therefore, surface damage limits can be increased to levels far greater than the SBS, SRS, and thermal limitations.

4 Conclusions

As MIR sources continue to demonstrate higher output powers with improvements in beam quality, it will be highly desirable to enable fiber transmission of such sources. ChGs cover a broad MIR (1 to 12 μm) window; however, they suffer from poor mechanical properties. To combat this, mechanically robust ChG fibers have been drawn and demonstrated power handling >10 W at 2053 nm. The ChG fibers were AR-coated, enabling >90% transmission through 20-cm length fibers. However, the AR-coatings were the primary failure mechanism via cracking after high power exposure. If AR microstructures are applied, or if AR-coatings are avoided, there is still the question of other effects on power handling capacity of single-mode ChG fibers. The primary limitations are SBS, SRS, and thermal

failure. Overall, SBS is the prime factor limiting power handling of single frequency beams in ChG fibers that are more than a meter long. For example, SBS will limit power handling to ∼1 W through a 1-m length of fiber, but can be avoided by using a spectrally broadband source. For broadband sources, power handling is limited by either heating effects or SRS; which one is dominant depends on the details of incident power, passive loss, core size, wavelength, and heat transfer rate. Chalcogenide fibers should be capable of ≥100-W beam transport with use of low-loss fibers and efficient heat removal.

Acknowledgments

We gratefully acknowledge the fiber polishing and coating efforts of Anthony Riggins and Ahmed El Halawany as well as helpful discussions with Lawrence Shah. We also acknowledge funding from the National Science Foundation (NSF) (1500292 Partnerships of Innovation: Accelerating Innovation Research Technology Translation). The authors have no relevant financial interests in the paper and no other potential conflicts of interest to disclose.

References

1. S. Mirov et al., "Frontiers of mid-IR lasers based on transition metal doped chalcogenides," *IEEE J. Sel. Top. Quantum Electron.* **24**(5), 1–29 (2018).
2. D. J. Creeden et al., "High power mid-infrared laser sources," in *Conf. on Lasers and Electro-Optics*, p. ATh3K.1 (2016).
3. F. Maes et al., "5.6 W monolithic fiber laser at 3.55 μm," *Opt. Lett.* **42**(11), 2054–2057 (2017).
4. V. Fortin et al., "30 W fluoride glass all-fiber laser at 2.94 μm," *Opt. Lett.* **40**(12), 2882–2885 (2015).
5. P. Figueiredo et al., "Progress in high-power continuous-wave quantum cascade lasers [Invited]," *Appl. Opt.* **56**(31), H15–H23 (2017).
6. G. Tao et al., "Infrared fibers," *Adv. Opt. Photonics* **7**(2), 379–458 (2015).
7. E. A. Romanova et al., "Multimode chalcogenide fibers for evanescent wave sensing in the Mid-IR," *IEEE J. Sel. Top. Quantum Electron.* **23**(2), 289–295 (2017).
8. F. Starecki et al., "Infrared sulfide fibers for all-optical gas detection," *Proc. SPIE* **10528**, 105280H (2018).
9. B. Bureau et al., "Chalcogenide optical fibers for mid-infrared sensing," *Opt. Eng.* **53**(2), 027101 (2014).
10. E. A. Anashkina et al., "Development of As-Se tapered suspended-core fibers for ultra-broadband mid-IR wavelength conversion," *J. Non-Cryst. Solids* **480**, 43–50 (2018).
11. C. R. Petersen et al., "Mid-infrared supercontinuum covering the 1.4 – 13.3 μm molecular fingerprint region using ultra-high NA chalcogenide step-index fibre," *Nat. Photonics* **8**, 830–834 (2014).
12. J. Tang et al., "$As_{40}S_{59}Se_1/As_2S_3$ step index fiber for 1 – 5 μm supercontinuum generation," *J. Non-Cryst. Solids* **450**, 61–65 (2016).
13. S. Xing et al., "Mid-infrared continuous-wave parametric amplification in chalcogenide microstructured fibers," *Optica* **4**(6), 643–648 (2017).
14. Z. Tang et al., "Low loss Ge-As-Se chalcogenide glass fiber, fabricated using extruded preform, for mid-infrared photonics," *Opt. Mater. Express* **5**(8), 1722–1737 (2015).
15. G. E. Snopatin et al., "High-purity chalcogenide glasses for fiber optics," *Inorg. Mater.* **45**(13), 1439–1460 (2009).
16. L. Sójka et al., "Numerical and experimental investigation of mid-infrared laser action in resonantly pumped Pr^{3+} doped chalcogenide fibre," *Opt. Quantum Electron.* **49**(1), 21 (2017).
17. L. Sojka et al., "Mid-infrared emission in Tb^{3+}-doped selenide glass fiber," *J. Opt. Soc. Am. B* **34**(3), A70–A79 (2017).
18. F. Starecki et al., "8 μm luminescence from a Tb^{3+} GaGeSbSe fiber," *Opt. Lett.* **43**(6), 1211–1214 (2018).
19. S. Shabahang et al., "Robust multimaterial chalcogenide fibers produced by a hybrid fiber-fabrication process," *Opt. Mater. Express* **7**(7), 2336–2345 (2017).
20. A. Sincore et al., "High power single-mode delivery of mid-infrared sources through chalcogenide fiber," *Opt. Express* **26**(6), 7313–7323 (2018).
21. J. Sanghera et al., "Reduced Fresnel losses in chalcogenide fibers by using anti-reflective surface structures on fiber end faces," *Opt. Express* **18**(25), 26760–26768 (2010).
22. I. Scripachev et al., "Optical and mechanical characteristics of fibers made of arsenic chalcogenides," *J. Optoelectron. Adv. Mater.* **3**(2), 351–360 (2001).
23. IRFlex Corporation, "IRF-S series chalcogenide mid-wave infrared fiber," 2018, https://www.irflex.com/products/irf-s-series/
24. Coractive, "IR fibers," 2016, http://coractive.com/products/mid-ir-fibers-lasers/ir-fibers/index.html
25. P. Zhang et al., "Fabrication of chalcogenide glass photonic crystal fibers with mechanical drilling," *Opt. Fiber Technol.* **26**, 176–179 (2015).
26. Q. Coulombier et al., "Casting method for producing low-loss chalcogenide microstructured optical fibers," *Opt. Express* **18**(9), 9107–9112 (2010).
27. J. S. Sanghera, L. B. Shaw, and I. D. Aggarwal, "Chalcogenide glass-fiber-based Mid-IR sources and applications," *IEEE J. Sel. Top. Quantum Electron.* **15**(1), 114–119 (2009).
28. A. Sincore et al., "SBS threshold dependence on pulse duration in a 2053 nm single-mode fiber amplifier," *J. Lightwave Technol.* **35**(18), 4000–4003 (2017).
29. F. Chenard, O. Alvarez, and A. Buff, "Mid-infrared chalcogenide fiber devices for medical applications," *Proc. SPIE* **10488**, 104880S (2018).
30. D. S. Hobbs, "Laser damage threshold measurements of anti-reflection microstructures operating in the near UV and mid-infrared," *Proc. SPIE* **7842**, 78421Z (2010).
31. S. Sato et al., "Multihundred-watt CO laser power delivery through chalcogenide glass fibers," *Appl. Phys. Lett.* **62**(7), 669–671 (1993).
32. K. Ogusu, H. Li, and M. Kitao, "Brillouin-gain coefficients of chalcogenide glasses," *J. Opt. Soc. Am. B* **21**(7), 1302–1304 (2004).
33. C. Florea et al., "Stimulated Brillouin scattering in single-mode As_2S_3 and As_2Se_3 chalcogenide fibers," *Opt. Express* **14**(25), 12063–12070 (2006).
34. G. P. Agrawal, *Nonlinear Fiber Optics*, 4th ed., Academic Press, Burlington, Massachusetts (2007).
35. R. Pant et al., "On-chip stimulated Brillouin scattering," *Opt. Express* **19**(9), 8285–8290 (2011).
36. A. Kobyakov, M. Sauer, and D. Chowdhury, "Stimulated Brillouin scattering in optical fibers," *Adv. Opt. Photonics* **2**(1), 1–59 (2010).
37. R. G. Smith, "Optical power handling capacity of low loss optical fibers as determined by stimulated Raman and Brillouin scattering," *Appl. Opt.* **11**(11), 2489–2494 (1972).
38. O. P. Kulkarni et al., "Third order cascaded Raman wavelength shifting in chalcogenide fibers and determination of Raman gain coefficient," *Opt. Express* **14**(17), 7924–7930 (2006).
39. M. Asobe et al., "Third-order nonlinear spectroscopy in As_2S_3 chalcogenide glass fibers," *J. Appl. Phys.* **77**(11), 5518–5523 (1995).
40. L. Schneebeli et al., "Measurement of the Raman gain coefficient via inverse Raman scattering," *J. Opt. Soc. Am. B* **30**(11), 2930–2939 (2013).
41. D. Mahgerefteh et al., "Technique for measurement of the Raman gain coefficient in optical fibers," *Opt. Lett.* **21**(24), 2026–2028 (1996).
42. J. S. Sanghera and I. D. Aggarwal, "Active and passive chalcogenide glass optical fibers for IR applications: a review," *J. Non-Cryst. Solids* **256–257**, 6–16 (1999).
43. Amorphous Materials Inc., "AMTIR-6 (As_2S_3) data sheet," 2018, http://www.amorphousmaterials.com/app/download/6552919404/AMTIR-6+Information.pdf
44. H. L. Lee et al., "Thermal conductivity improvement of surface-enhanced polyetherimide (PEI) composites using polyimide-coated h-BN particles," *Phys. Chem. Chem. Phys.* **16**(37), 20041–20046 (2014).
45. Plastics International, "Ultem(r) polyetherimide data sheet," 2018, https://www.plasticsintl.com/datasheets/ULTEM_GF30.pdf

Alex Sincore received his BS degree in physics from the University of Florida in 2012. He went on to receive his MS degree in optics from CREOL, the College of Optics and Photonics at the University of Central Florida in 2014. He is currently a PhD candidate in the optics program at CREOL. Since 2012, he has been a graduate research assistant in the Laser Plasma Laboratory. His primary research interests are in designing and developing high-power and high-energy fiber lasers. His additional research interests include applications in material processing and atmospheric propagation, nonlinear effects in optical fibers, and nonlinear frequency conversion to the midinfrared.

Justin Cook received his BS degree in physics and applied mathematics from Austin Peay State University in 2015, and his MS degree in optics and photonics from the CREOL, the College of Optics and Photonics, University of Central Florida, Orlando, USA, in 2017, where he is currently working toward his PhD in the optics program. His interests include developing high-power fiber lasers for material processing and nonlinear optical applications.

Felix Tan is a PhD candidate in optics at CREOL, the College of Optics and Photonics, University of Central Florida. He earned his BS degree in physics from the University of Florida and his MS degree in optics from UCF. His research focuses on the fabrication and

characterization of multimaterial, multifunctional cables, fibers, and fabrics. He is particularly interested in the design and implementation of related equipment and machinery, along with the transition from laboratory-scale prototypes and processes to production-scale systems and operations. He plans to defend and graduate in the fall of 2018.

Ayman F. Abouraddy is a professor of optics and photonics at CREOL, the College of Optics and Photonics, University of Central Florida. He received his BSc and MSc degrees from Alexandria University, Alexandria, Egypt, and his PhD from Boston University, Boston, Massachusetts, USA. He carries out research in the area of multimaterial fibers, spatiotemporal optical field synthesis, non-Hermitian photonics, and quantum optics.

Martin C. Richardson: Biography is not available.

Kenneth L. Schepler is a research professor at CREOL, the College of Optics and Photonics, University of Central Florida. He received his BS degree in physics from Michigan State University and his MS and PhD degrees in physics from the University of Michigan. He currently conducts research on the development of fiber and waveguide-based infrared laser sources. He is a fellow of the Optical Society of America and of the Air Force Research Laboratory.